

Article

Investigation of Gliding Walled Multilayer Waveguides

Mohsin Ali Shah Syed ¹, Junsheng Yu ^{2,3,4,*}, Yuan Yao ¹ and Shanzah Shaikh ⁵

¹ School of Electronic Engineering, Beijing University of Posts and Telecommunications, Beijing 100876, China; mohsin@bupt.edu.cn (M.A.S.S.); yaoy@bupt.edu.cn (Y.Y.)

² BUPT-QMUL EM Theory and Application International Research Lab, Beijing University of Posts and Telecommunications, Beijing 100876, China

³ School of Physics and Electronic Information, Anhui Normal University, Wuhu 241000, China

⁴ School of Intelligence and Digital Engineering, Luoyang Vocational College of Science and Technology, Luoyang 471023, China

⁵ Department of Telecommunication Engineering, Mehran University of Engineering and Technology, Jamshoro 76062, Pakistan; shanzah.shaikh@faculty.muet.edu.pk

* Correspondence: jsyu@bupt.edu.cn

Abstract: This article suggests a new waveguide design that utilizes a “walled” architecture. Instead of relying on conventional gap waveguide structures to create electronic bandgaps and prevent field leakage, the proposed design introduces a “walled” guiding mechanism. This technique preserves transmission while maintaining the multilayer approach and eliminates the need for nails or chemical bonds to attach the layers. Simulations were carried out in the W-band (75–110 GHz) and D-band (110–170 GHz) using several metals, and measurements were performed in the W-band using aluminum. The simulation results show that the reflection coefficient was less than -40 dB over the entire D-band. At the same time, the average insertion loss was around 0.0054 dB/mm and around 0.0065 dB/mm for silver and gold, respectively. Similarly, the reflection coefficient was less than -45 dB over the 75–110 GHz range, with an average insertion loss of 0.0018 dB/mm for silver and 0.003 dB/mm for gold, respectively. The aluminum model’s reflection coefficient was less than -35 dB, and the average insertion loss was 0.0035 dB/mm. The experimental results achieved a reflection coefficient of less than -30 dB and the average transmission coefficient was -0.2 dB, with an insertion loss of 0.002 dB/mm. The simple stacking ability of the weightless walled metal plates and easy fabrication makes the proposed transmission line a promising technology in mmWave and Terahertz applications.

Keywords: multi-layer waveguides (MLWs); terahertz; interlocking; guiding; gliding; walled MLW; sliding; bed of nails; glide symmetry; electronic band gap (EBG); stack



Citation: Shah Syed, M.A.; Yu, J.; Yao, Y.; Shaikh, S. Investigation of Gliding Walled Multilayer Waveguides. *Electronics* **2024**, *13*, 599. <https://doi.org/10.3390/electronics13030599>

Academic Editors: Ke Guan, Hao Jiang, Yong Niu and Zhipeng Lin

Received: 18 December 2023

Revised: 28 January 2024

Accepted: 29 January 2024

Published: 1 February 2024



Copyright: © 2024 by the authors. Licensee MDPI, Basel, Switzerland. This article is an open access article distributed under the terms and conditions of the Creative Commons Attribution (CC BY) license (<https://creativecommons.org/licenses/by/4.0/>).

1. Introduction

In recent years, the rapid advancement of next-generation wireless communication has led to increased significance of the millimeter-wave frequency band, attributed to its abundant spectrum, expansive bandwidth, and capacity for enabling mmWave circuits. Millimeter-wave circuits and modules are crucial for wireless front-end systems, requiring high performance, low loss, and cost-effectiveness. Planar transmission lines like microstrip lines and coplanar waveguides offer easy integration with other circuits for affordable and compact designs. However, their mmWave application is hampered by high insertion loss and radiation loss. Hollow rectangular and cylindrical waveguides are primarily used for their low loss and high-power capabilities, but incorporating their structure with other passive and active planar circuits poses challenges [1–3].

Gap waveguide (GWG) technology has recently gained attention as a potential interconnection for millimeter-wave applications. Pioneered by Kildal et al., the concept of GWG was developed on soft and hard surfaces. The original GWG setup utilized periodic pins as a perfect magnetic conductor (PMC), meaning that electromagnetic waves cannot

travel between a PMC plate and a perfect electric conductor (PEC) plate until a propagation path is established. Essentially, the GWG can be seen as an electromagnetic bandgap (EBG) transmission structure where, at specific frequencies, electromagnetic waves are not allowed to propagate within the EBG area. Instead, they must follow an established propagation path [4]. Several types of unit cells for GWGs have been proposed, including the initial “bed-of-nails” pin unit cells, half-height pin unit cells, interdigital pin unit cells, and a glide symmetric holey unit cell. An embedded pin unit cell was also introduced to enhance the working bandwidth and frequency performance [5–7]. The initial designs involved the use of EBGs, which required at least two rows of pins along the transmission line paths to minimize electromagnetic field leakage. Many devices and mmWave components were manufactured utilizing these pin-based unit cells, such as bandpass filters [8], D-band slot antenna array [9], horn antennas [10], Luneburg antennas [11], and other gap waveguide-based components [12–18]. However, as mentioned in [7], the disadvantage of manufacturing these nails or pins was the complexity of producing them on the mm and μm scale. Moreover, if the pins were thin, they could easily break during the manufacturing process. Various approaches were proposed to address this issue. One suggested idea was to remove the pins altogether and then incorporate holes, or rather, glide symmetric holes [7], to achieve the same effect as the pin unit EBGs, although the holey EBGs provided better broadband performance [19]. The effect of the shape of the holes was also quite extensively studied in [20–24]. Suggestions also involved replacing CNC-based manufacturing techniques with other manufacturing techniques such as additive manufacturing (material jetting, binder jetting and nanoparticle jetting) and 3D printing [25–27] or methods based on subtractive manufacturing, such as electric discharge machining (EDM) or metal etching [12,13,16,28]. The exploration of periodic symmetries (or higher symmetries) first began in the 1960s [29], and with the development of computer simulation tools, there has been an increased focus on investigating periodic symmetries or higher symmetries. Research indicates that integrating glide symmetry into periodic structures results in decreased dispersion and improved electromagnetic bandgap reactions. However, the main challenge with gap waveguide technology lies in the arrangement of the intricate hole patterns and the difficulties associated with their implementation in millimeter wave devices [30–33].

Our paper introduces a novel multilayered configuration that offers a simplified guiding structure with minimal loss and easy mechanical assembly for millimeter-wave applications. The design is based on the stacking of plates, influenced by the approach proposed in [23] but without relying on periodic symmetries or a bed of nails. This layered structure prevents field leakage using walls and eliminates the need for unique patterns and complex fabrication methods, making assembly more straightforward. Moreover, our study includes the simulation of two straight multilayer waveguide (MLW) transmission lines operating at different frequency bands, namely, W-band (75–110 GHz) and D-band (110–170 GHz), and an aluminum W-band walled MLW waveguide with double 90° embedded H-plane bends. A prototype was also fabricated to validate the proposed concept, where the simulated W-band straight and bend transmission lines were manufactured by employing chemical metal etching on aluminum.

2. Walled Multilayer Waveguide Transmission Line Configuration and Design

Figure 1 represents the basic configuration of the proposed walled transmission line. In the multi-layered approach of gap waveguides, the layers do not have electrical or galvanic contact. Thus, the air gaps between the layers cause field leakage, as Figure 1a illustrates. The “periodic higher symmetry” and “bed of nails” types of gap waveguides were invented to prevent this leakage. In our proposed novel structure, the use of raised edges or “walls” was introduced along the path of the waveguide channel to achieve the same purpose, as depicted in Figure 1b. Unlike gap waveguides, where, to prevent the field leakage, a stopband needs to be created via pins or holes, the concept of our proposed structure is basically to incorporate walls along the length of the waveguide channel or path, which can prevent field leakage in the direction perpendicular to the

wave propagation. Thus, without the need for a pin or hole symmetry, the proposed structure can mimic the behavior of a conventional waveguide. Figure 2a,b show that the proposed waveguide dispersion diagram resembles the conventional W-band and D-band rectangular waveguide dispersion diagram for the simulated W- and D-band GW-MLW waveguides. Figure 2a depicts the W-band GWMLW unit cell with dimensions of $a_W = 1.27$ mm, $b_W = 2.54$ mm, and $l_W = 2$ mm, whereas Figure 2b shows the D-band GWMLW unit cell with dimensions of $a_D = 0.826$ mm, $b_D = 1.651$ mm, and $l_D = 1$ mm. The dispersion diagrams were calculated using CST Microwave Studio (2019) software Eigenmode solver. Furthermore, the dispersion diagrams depict the first three propagating modes for analysis. The reference unit cell shared identical dimensions with the respective band waveguide dimensions for consistency. Figure 2a illustrates that the dispersion diagram of the W-band GWMLW was identical to the ideal regular W-band waveguide for the propagating modes in consideration. Equally, in the D-band GWMLW, the modes displayed quite similar behavior to that of the D-band ideal regular waveguide, although not perfectly identical. Thus, it can be said that the proposed novel structure can be used in place of regular waveguides for mmWave applications.

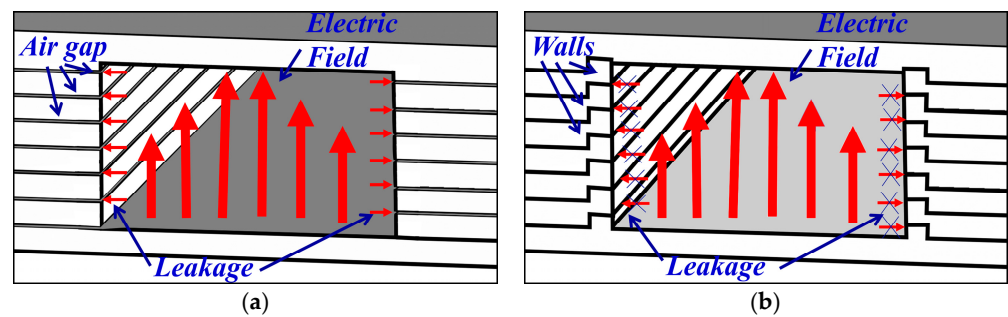


Figure 1. Configuration of the proposed MLW transmission line. (a) Cross-sectional view of an eight-layer waveguide with little air gaps in between. (b) The walled structure illustrates field leakage suppression.

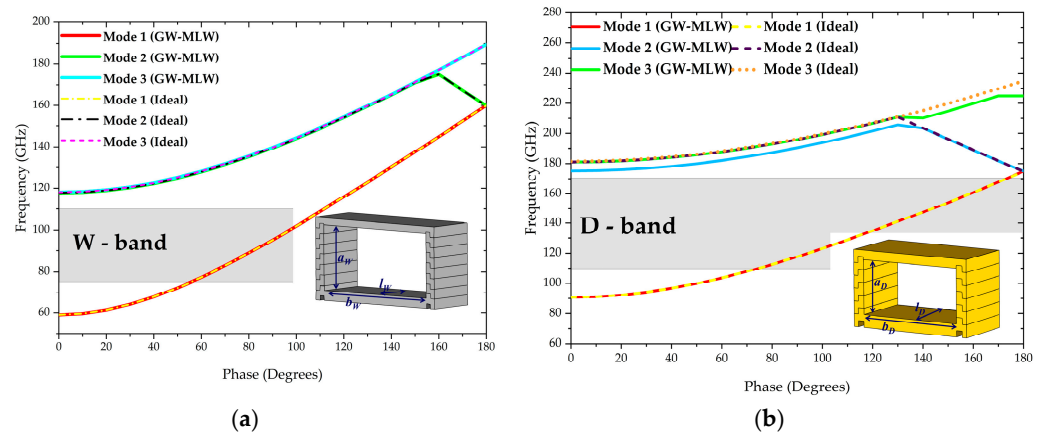


Figure 2. Dispersion diagrams of the proposed GW-MLW compared with ideal rectangular waveguides of the corresponding frequency bands. (a) W-band GW-MLW waveguide dispersion diagram compared with ideal W-band waveguide. (b) D-band GW-MLW waveguide compared with ideal D-band waveguide.

Like the aforementioned multi-layered waveguide designs, our proposed structure, shown in Figure 3a, also incorporates several metal plates or layers stacked on each other. These plates have the waveguide channel cut out in the center. The top and bottom plates provide cover to the waveguide channel. The proposed design is usable for all bands, wherein the intermediate layers have an elevated wall that provides the waveguide channel, and the top and bottom layers enclose the intermediary layers.

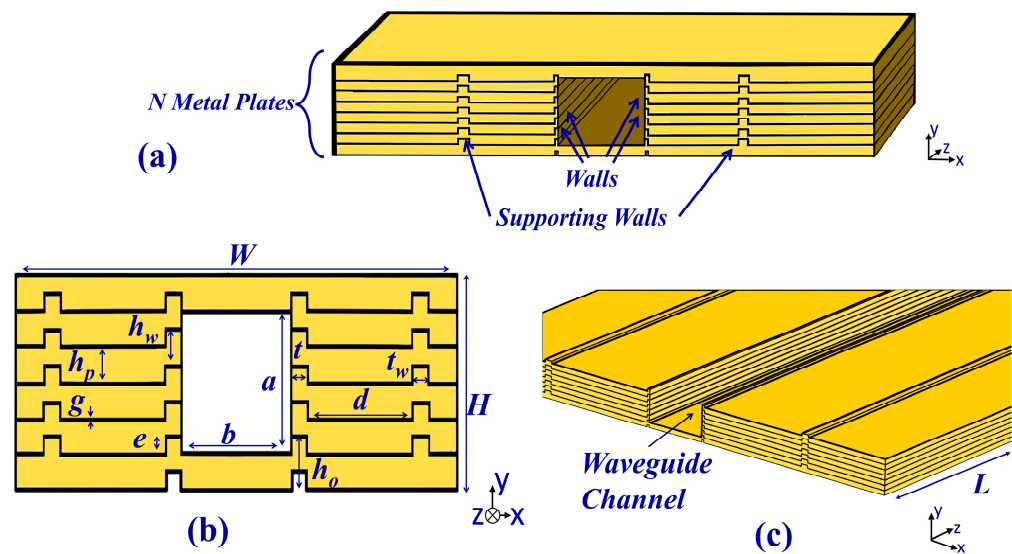


Figure 3. Configuration of the proposed walled multilayer waveguide transmission line. (a) Cross-sectional view of the layered concept with N metallic plates. (b) Dimensions used in the proposed MLW line. (c) Perspective view of the transmission line with the top layer removed and showing supporting walls.

These intermediary layers have walls on the ends facing the waveguide channel. The wall of the lower layer inserts into the edges of the upper layers. In other words, the groove of the upper layers is fitted into the ridge of the lower layers. This mechanism provides a means of interlocking the multiple layers. An additional pair of supporting walls is added on the far side of each layer to prevent the intermediary sides from slipping away from their positions, as depicted in Figure 3b,c. The inner walls run through the entire waveguide length and alongside the waveguide channel. The outer walls, however, do not necessarily have to follow the path of the waveguide channel.

Additionally, the bottom layer, or the “base,” has the wall raised on its topside, whereas the topmost layer, or the “cover,” has the pattern etched on its underside. All the layers can have the same pattern, which substantially benefits the fabrication phase of the waveguide. This method of stacking the walls may also remove the need to use screws or glue to fix the layers into place. Lastly, after stacking the layers, simply pressing the base and the cover with minimal pressure would complete the waveguide construction. Figure 3b shows a closeup of the configuration of the proposed transmission line.

The metal plates each have a height h_p and an initial gap g between them. The initial height h_o mm of the plates is 0.3 mm, which is reduced by the minimum depth value e to 0.2 mm at some sections of the design to provide space for the insertion of the lower layers. The walls have an equal height of h_w mm and thickness of t mm. For the symmetric design of the plates and the walls, the plate height and wall height are kept equal, i.e., $h_p = h_w$, throughout the complete structure. The minimum depth e is also fixed to remain at half the value of the wall height h_w , i.e., $e = 0.5 h_w$. It can also be seen in Figure 3b that aside from the top and bottom layers, the intermediary layers are in pairs. These pairs are symmetric in shape. When stacked on top of one another, the metal plates do not have any electrical or galvanic contact. Stacking the walls provides a much simpler and more effective way of preventing field leakages throughout the structure.

Furthermore, a wall of thickness t_w mm at either side of the layers is also placed to provide added stability to the structure. These walls have the simple utility of preventing the layers from sliding out from the sides. They are located at d mm from the edge of the inner walls. The notches for the walls also provide a reference point for the walls. It should be noted that these walls are placed some distance away from the waveguide channel, so they have negligible interference with the waveguide channel. In the final assembly, all the

layers slide on top of each other, where the wall of the bottom layer slides into the notch of the top layer.

2.1. D-Band Gliding Walled Multilayer Straight Waveguide

The D-band waveguide is designed based on WR-6.5 dimensions—precisely, $b = 1.651$ mm width by $a = 0.826$ mm height. In this configuration, the plates have a length L of 30 mm, equating to 15λ at 150 GHz, and the plate width W measures 16 mm. This design uses six ($N = 6$) layers of height h_w equal to 0.2 mm, including the base and cover, to achieve a total height H equal to 1.2 mm. The plate height h_o is initially kept at 0.3 mm but is reduced to 0.2 mm along the wall path by $e = 0.1$ mm from under the upper plate to allow the wall of the lower layer to fit into place in the upper plate—hence, the reduction in layer height. Table 1 summarizes the configuration parameters of the D-band gliding wall MLW design.

Table 1. Dimensions of the proposed D-band walled multilayer waveguide (units: mm).

Parameter	Value	Parameter	Value
a	0.826	d	4.35
b	1.651	h_o	0.3
e	0.1	h_w	0.2
L	30	H	1.2
t	0.1	W	16
t_w	0.3	N	6

2.2. W-Band Gliding Walled Multilayer Straight Waveguide

The specifications for the W-band waveguide model adhere to WR-10 waveguide dimensions, essentially $b = 2.54$ mm by $a = 1.27$ mm. This waveguide's length L is set at 50 mm, corresponding to approximately 15λ at 92.5 GHz, whereas the width W is kept at 20 mm. This design utilizes eight layers ($N = 8$) for its construction, producing an overall height H of 1.7 mm. The plate height is 0.3 mm, which is reduced to 0.2 mm to allow the walls to fit into the insertion grooves. This reduction is achieved via the fabrication process used. Therefore, six intermediary layers of 0.2 mm, a base of 0.2 mm, and a cover of 0.3 mm would be sufficient to provide the inner height dimensions of the W-band model. The values of the W-band MLW transmission line parameters are summarized in Table 2.

Table 2. The dimensions of the proposed W-band walled multilayer waveguide (units: mm).

Parameter	Value	Parameter	Value
a	1.27	d	4.065
b	2.54	h_o	0.3
e	0.1	h_w	0.2
L	50	H	1.7
t	0.1	W	20
t_w	0.3	N	8

2.3. W-Band Gliding Walled Multilayer Waveguide with Double 90° Bend

For further investigation into the performance of the proposed transmission line within more complex designs, a double 90° bend was simulated using aluminum. This design extends the straight MLW waveguide by incorporating two H-plane bends in opposite directions. Figure 4 illustrates the geometry of the proposed waveguide bend design. The overall configuration follows that of the aforementioned straight W-band MLW waveguide but with additional H-plane bends following the optimized bend structures discussed in [34]. The total length L_a of the waveguide channel is 55.22 mm, corresponding to 17λ at 92.5 GHz, whereas the height of the structure is 1.7 mm. The optimized values of the three steps used in the design are $d = 0.569$ mm, $e = 0.909$ mm, and $f = 0.363$ mm. Table 3 lists the values of the parameters used in this structure's geometry.

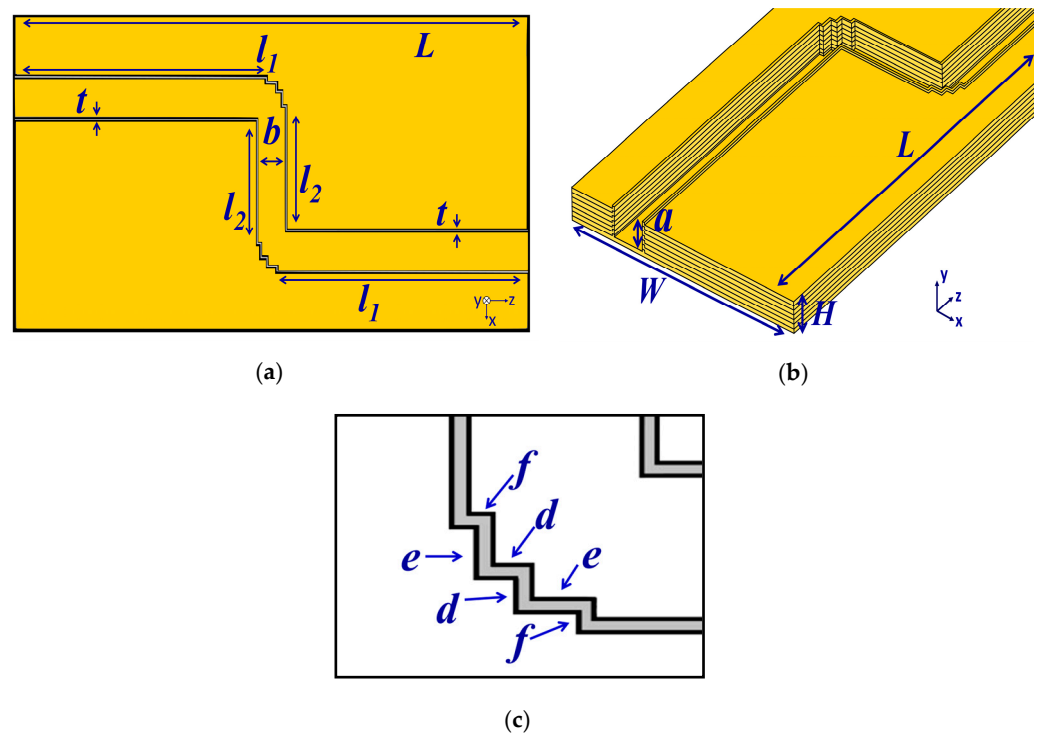


Figure 4. Top view of the proposed double 90° bend W-band multilayer waveguide. (a) Cover removed to show the inner dimensions of the bends. (b) Perspective view of the double 90° bend waveguide structure. (c) Close-up view of the three-stepped H-plane bend with step parameters.

Table 3. The dimensions of the proposed double 90° bend W-band walled multilayer waveguide (units: mm).

Parameter	Value	Parameter	Value
a	1.27	f	0.363
b	2.54	l ₁	23.53
e	0.909	l ₂	8.159
d	0.569	W	30
t	0.2	L _a	55.22
H	1.7	L	50

3. Simulation and Fabrication Results

3.1. Simulation Results

Simulations were performed for three waveguide configurations, i.e., two straight MLW transmission lines, one for the D-band, another for the W-band, and one double 90° bend W-band line, using CST Microwave Studio in all simulations. The findings are discussed below.

3.1.1. D-Band Gliding Walled Multilayer Straight Waveguide

The D-band GW-MLW line was simulated with silver as the conducting material. It was compared with an ideal rectangular waveguide (RW) of the same length, material, and standard inner dimensions. It is worth mentioning that the ideal RW equates to the GW-MLW with a zero mm air gap parameter-wise. The simulated reflection coefficients were less than −58 dB for the ideal rectangular waveguide (RW) and the GW-MLW for the whole D-band, respectively, as observed in Figure 5. The simulated transmission coefficient values were better than the −0.14 dB on average, as the figure shows. It indicates that the GW-MLW performed comparably to an ideal rectangular waveguide in an ideal scenario.

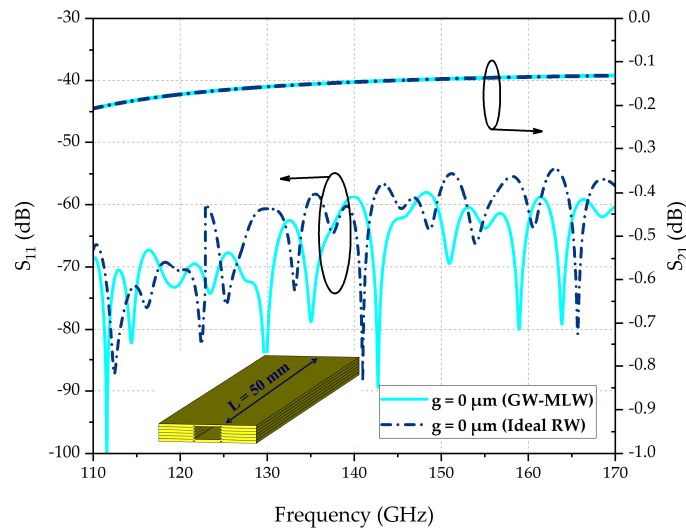


Figure 5. Simulated performance of the proposed D-band GW-MLW compared with the ideal RW.

Figure 6 compares the scenario of the simulated reflection and transmission coefficients of the D-band MLW when gold and silver were used as conducting materials. In this scenario, a gap of $g = 10 \mu\text{m}$ was also introduced in all the layers. There was a slight difference in the reflection performance when the materials were changed. However, the transmission coefficient performance was 0.05 dB better in gold than in silver. There was only a slight difference in the two material performances of around 0.1 dB for the reflection coefficient on average and of 0.04 dB for the transmission coefficient.

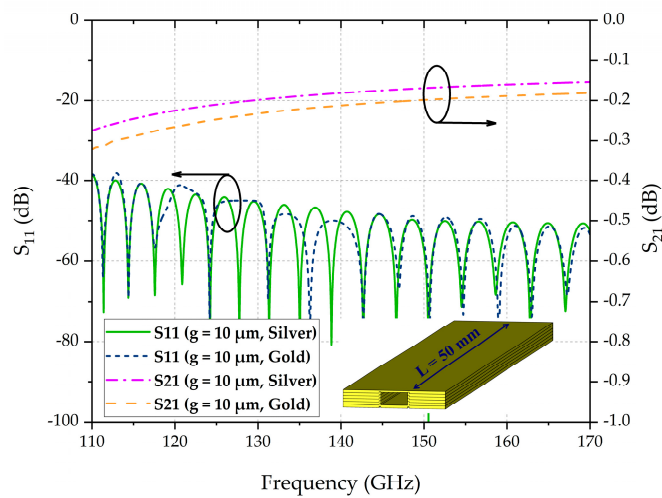


Figure 6. Transmission and reflection coefficients of the proposed GW-MLW for the D-band with gold and silver as conducting materials.

Figure 7a,b display the attenuation and phase constant graphs for the D-band GW-MLW, respectively, for silver and gold GW-MLW. The average attenuation constant was approximately 0.0054 dB/mm and 0.0046 across the entire frequency range for silver and gold, respectively, whereas the average phase constant measured 0.68 rads/m for both materials.

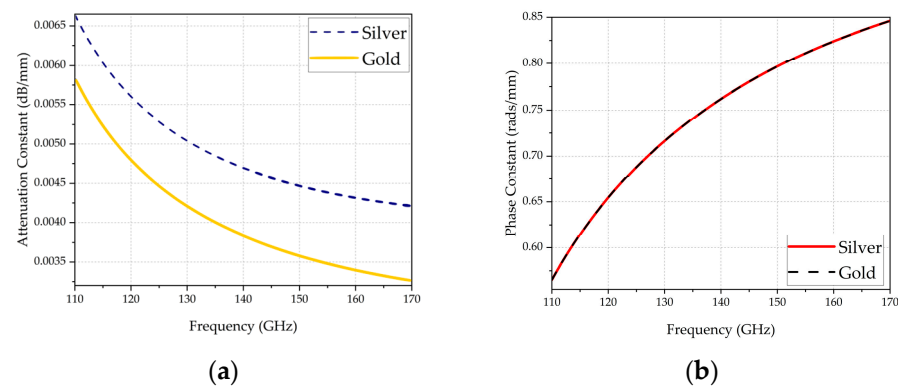


Figure 7. Simulated D-band GW-MLW. (a) Attenuation constant. (b) Phase constant.

3.1.2. W-Band Gliding Walled Multilayer Straight Waveguide

The simulated performance of the aluminum W-band GW-MLW compared with an ideal waveguide is shown in Figure 8. The GW-MLW was compared with the ideal RW when its gap $g = 0$ mm. The reflection coefficient values were less than -55 dB throughout the whole band for both the ideal waveguide and the GW-MLW. Also, the transmission coefficients for both waveguides showed a near-identical trend that averaged -0.14 dB for $g = 0$ μm in the GW-MLW. Thus, the behavior of the proposed GW-MLW waveguides resembles the ideal waveguides in ideal conditions.

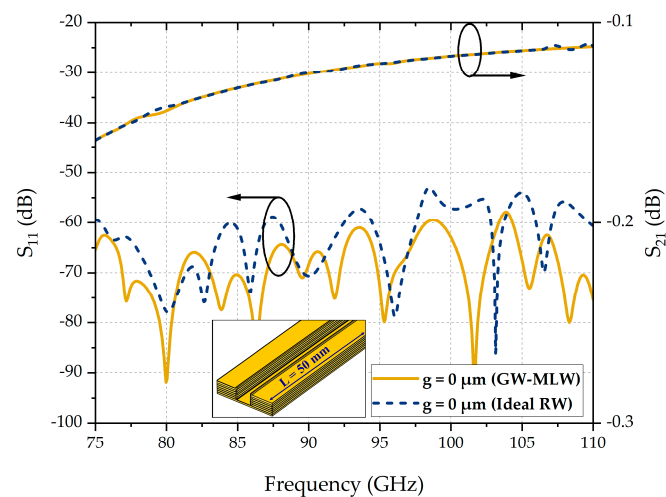


Figure 8. Simulated performance of the proposed W-band GW-MLW in comparison with the ideal RW.

Figure 9 compares the simulated reflection and transmission coefficients in the W-band GW-MLW when gold and silver were utilized as the conducting materials along with aluminum. A gap of $g = 10$ μm was inserted into all layers to assess the impact of air gaps. The reflection coefficient for silver was approximately -6 dB lower than that of gold across a significant portion of the W-band. In comparison, gold outperformed silver by 0.03 dB in terms of transmission coefficient performance. Meanwhile, the reflection parameter for aluminum had the highest loss of the three materials of around -25 dB over the whole band. Its transmission parameter, however, was the lowest of the three materials, averaging around -0.25 dB. The results presented in Figure 9 highlight the noticeable disparities in the reflection and transmission coefficients of the W-band GW-MLW when using gold, silver, and aluminum.

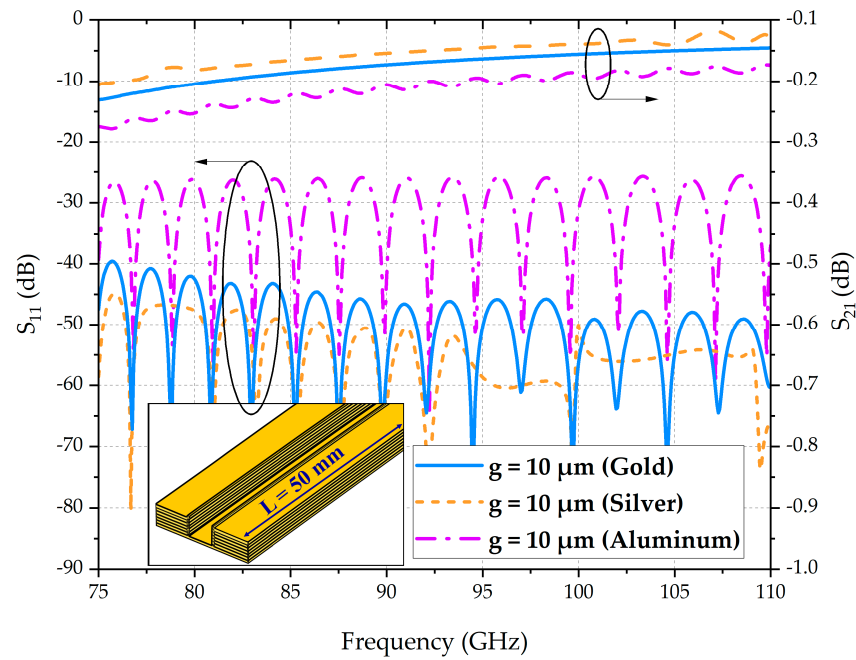


Figure 9. Simulated performance of the proposed GW-MLW for the W-band with gold and silver with a gap of 10 μm between the layers.

Figure 10a,b compare the attenuation and phase constant graphs for the W-band GW-MLW. The average attenuation constant of silver was approximately 0.002 dB/mm less than that of aluminum across the entire frequency range. In contrast, the average phase constant of silver was nearly identical to that of aluminum, measuring 0.732 rads/mm on average in the entire frequency band. The attenuation constant of gold, being 0.0032 dB/mm, however, was close to that of aluminum (0.0035 dB/mm) across the W-band. The inset in Figure 10b shows a minute difference between the phase constant values for silver, aluminum, and gold in the GW-MLW, with the values of silver and gold being identical in the same frequency band.

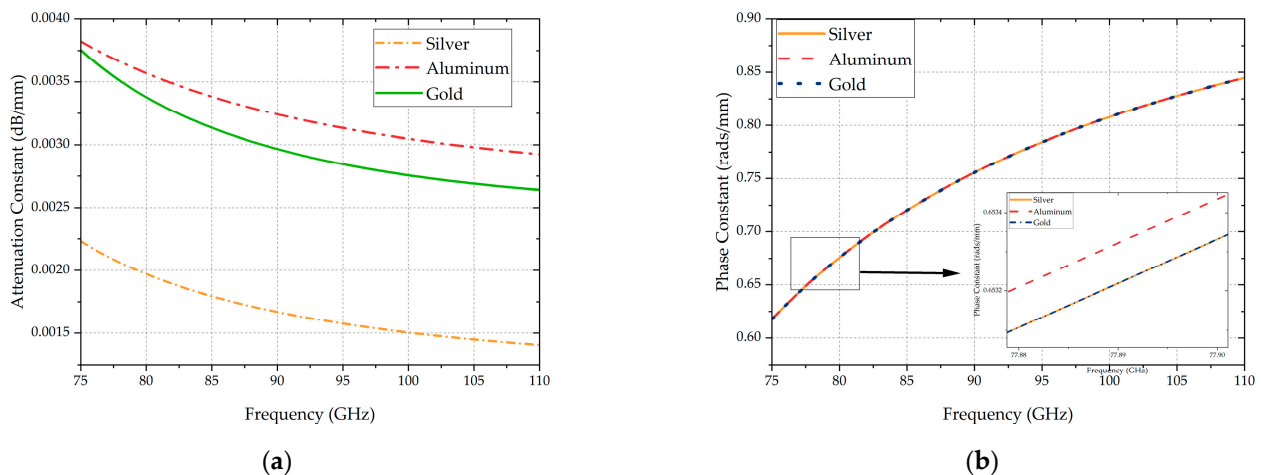


Figure 10. Simulated W-band GW-MLW comparisons of silver, gold, and aluminum. (a) Attenuation constant. (b) Phase constant. (Inset: closeup of phase constant showing approximately equal curves).

3.1.3. W-Band Gliding Walled Multilayer Waveguide with Double 90° Bend

The comparison of the transmission and reflection coefficients of the double 90° bend GW-MLW waveguide with an ideal RW is represented in Figure 11. The ideal waveguide reflection coefficient was less than -25 dB throughout the frequency band, whereas the

GW-MLW was -40 dB across the same band. Additionally, the transmission coefficient of the GW-MLW was -0.22 dB, whereas the ideal waveguide was -0.21 dB in the same frequency range, as observed in Figure 11b. The GW-MLW and ideal waveguide transmission coefficient parameters differed by 0.01 dB over a large portion of the frequency band.

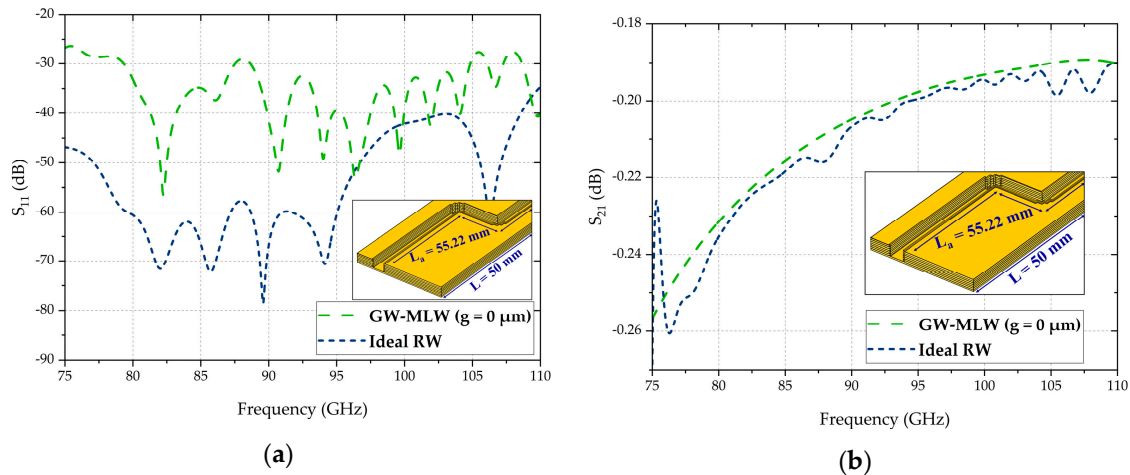


Figure 11. Comparison of the S parameters of the GW-MLW and the ideal RW with a double 90° bend in W-band showing (a) Reflection coefficient (b) Transmission coefficient.

3.2. Sensitivity and Tolerance Analysis

A sensitivity analysis was carried out that was centered on examining the impacts of deviations in the physical dimensions of the proposed waveguide. It encompassed variations in the wall height, thickness, and air gap width between the plates. In doing so, we included all possible options in an actual fabrication process. The different physical dimensions were generated sequentially via a parametric sweep using the CST Microwave Studio software. The tolerance values provided by the manufacturer were ± 2 μm in width and height. At the same time, the airgap produced by plate flatness and misalignment of the walls could only be estimated by varying the values from 0 mm (no air gap) to 0.1 mm (half of the wall height), as beyond this upper-limit value, the structure ceases to perform as intended. The structure ceases to function because the wall etching is 0.1 mm on the lower layer and 0.1 mm on the groove for the wall in the upper layer; therefore, when the air gap difference is more than 0.1 mm, the field spreads within the structure. It is noted that in similar configurations of the walled MLW, the etching depth plays a vital role in the performance of the proposed structure. Simulations were performed for each combination of errors. Therefore, the effects of the combinations were observed and are discussed in the subsequent section below.

(a) W-band straight GW-MLW

The sensitivity analysis of the proposed transmission line was performed while considering the parameters mentioned above. Figure 12a,b depict the fluctuations in the reflection and transmission coefficients, respectively, of the straight GW-MLW waveguide when the height and width of the wall and the air gap were varied as per the manufacturing tolerance value. Figure 12a shows that the reflection coefficients followed a similar trend throughout the variations. The response was less than -40 dB throughout the entire frequency band when the air gap was 0.002 mm. However, at frequencies above 95 GHz, the fluctuations varied rapidly when the air gap reached the maximum gap of 0.1 mm. Consequently, due to the air gap corridors that formed, fluctuations appeared in both coefficients, especially after the air gap value of 0.05 mm. Figure 12b highlights the simulation of the response fluctuation for a gap value of 0.07 mm, although for lesser air gap values the response of the structure was satisfactory. Figure 12c shows the concept of the air gap corridor that was created when the manufacturing tolerance produced gaps between the walls.

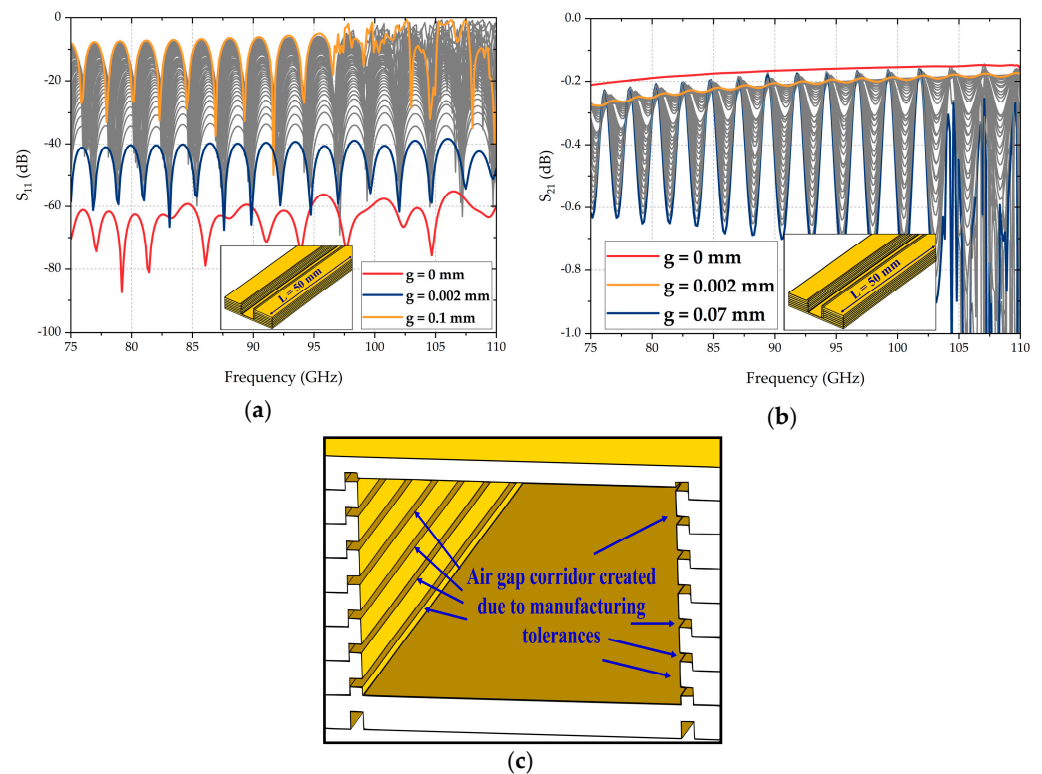


Figure 12. Tolerance analysis of the W-band straight GW-MLW by varying the parameter g . (a) Reflection coefficient. (b) Transmission coefficient. (c) Depiction of the air gap corridor formed due to manufacturing tolerances.

(b) W-band double-bend GW-MLW

Sensitivity analysis results of the W-band GW-MLW double-bend waveguide are analyzed in Figure 13. As in the above section, the wall height, thickness, and air gap parameters varied from 0 mm to 0.1 mm using the tolerance value provided by the manufacturer. It can be observed in Figure 13a that there were many fluctuations in the reflection parameter response, although the maximum value of these fluctuations was no more than -15 dB. Even for the maximum value of the air gap (i.e., 0.1 mm), the losses were less than -25 dB throughout the frequency band. In Figure 13b, it is evident that the transmission coefficient was also affected by the changes in the physical parameters of the simulated structure, although the losses were between -0.2 dB and -1 dB in the frequency band.

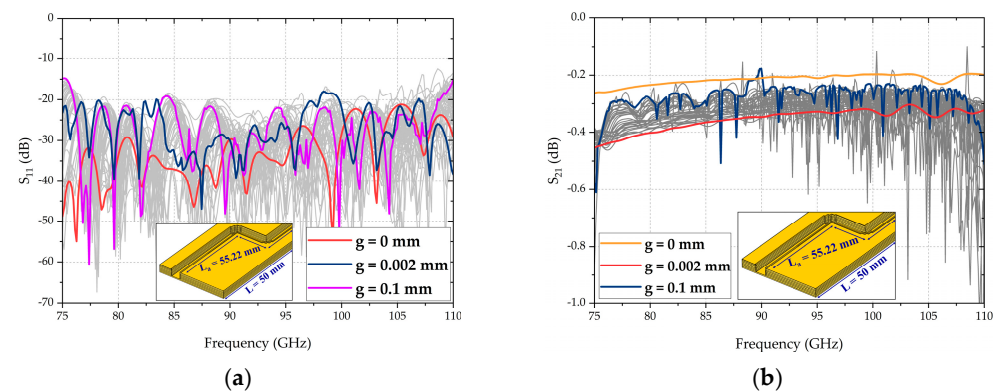


Figure 13. Tolerance analysis of the W-band double-bend GW-MLW by varying the parameter g . (a) Reflection coefficient. (b) Transmission coefficient. The gray lines represent various ranges of coefficients that exhibit acceptable levels of performance.

3.3. Fabrication and Results

Both the straight and the double 90° bend simulated aluminum W-band GW-MLWs presented in the above sections were fabricated to validate the performance and provide proof of concept. A single integrated waveguide that stacked eight layers of the waveguide structure was manufactured, as represented in Figure 14. This step brought about three pieces of each intermediary layer. However, the base and cover layers were manufactured as single pieces, as seen in Figure 14a. All the layers were manufactured with the chemical metal-etching process. This low-cost process is a corrosion process commonly used to manufacture complex metallic structures. The layers were etched twice with an etch depth of 0.1 mm, once below and then above, on a standard aluminum sheet with a thickness of 0.3 mm, yielding a minimum thickness of 0.2 mm at the intended segments of the layers. The conventional UG-387/U flange clefs were incorporated on the layer's sides to provide a proper flange connection to the GW-MLW, as observed in Figure 14c. Aluminum flange fixtures that provide flange connections to the GW-MLW were also manufactured. Guiding holes and screw threads were drilled onto the prototype and the fixtures, after which the layers were polished and the waveguide interface was smoothed. It is worth mentioning that the screws had not been fixed along the waveguide length since the inherent wall design of the prototype only used the dowels and the flange fixtures to fix the layers into place. Firstly, the lower flange support was positioned, followed by the base. Subsequently, the layers were sequentially stacked on top of each other before placing the cover. Next, the upper flange support was added on top, and dowels were inserted into the alignment holes. Finally, the flange supports were fastened together with screws. The walls of the double-bend waveguide acted as supporting walls of the straight waveguide, preventing the top layer from moving out of position after being stacked. Likewise, the walls of the straight waveguide acted as the supporting walls of the double-bend waveguide.

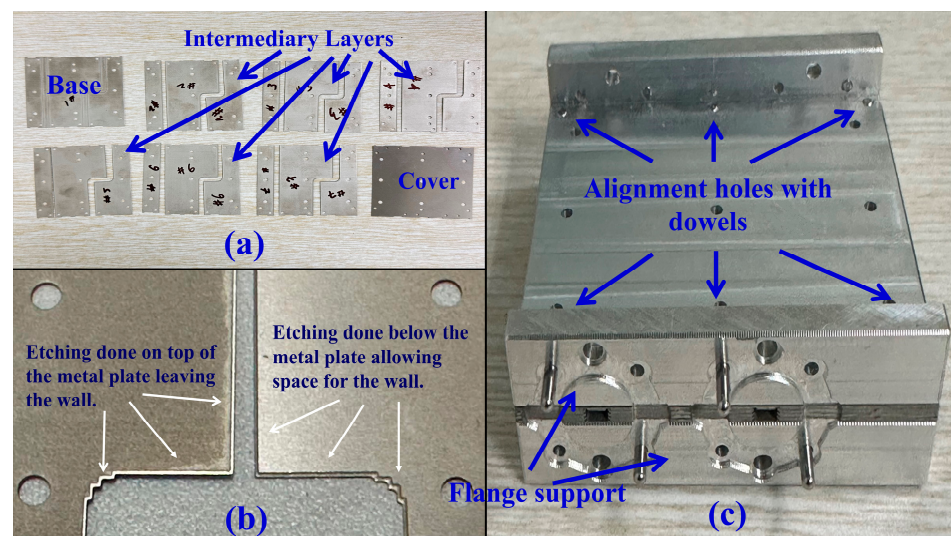


Figure 14. Photograph of the GW-MLW prototype fabricated via the metal-etching process. (a) Three pieces each of the intermediary layers and single pieces of the base and cover layers. (b) Close-up view of the etched top and bottom of the metal plates. (c) Final assembly of the gliding walled MLW.

The manufacturing tolerance was $\pm 2 \mu\text{m}$ of the metal thickness, hence becoming $\pm 0.66\%$ for metal sheets of 300 μm or 0.3 mm. The surface roughness of the fabricated prototype was 0.8 μm , which was included in the simulations. The lower and upper flange attachments were screwed together, sandwiching the GW-MLW, and then measurements were carried out. Moreover, the stacking was carried out without the application of any adhesive. However, alignment dowel screws were employed to ensure accurate positioning between all the plates, including the flange attachments. The fabricated prototype was tested using Keysight VNA N5247B. The integrated prototype was excited using conven-

tional W-band flange adaptors and transitions. Since there were no E-plane bends or transitions in the structure, this adds to the advantages of the proposed structure. The measurement of the air gap between the prototype was not controlled, although every effort was taken to keep it as close to zero millimeters as possible.

The measured and simulated performance of the straight GW-MLW waveguide can be observed in Figure 15. Figure 15a shows that the straight waveguide's measured reflection coefficient was less than -20 dB in the W-band frequency range, whereas the simulated reflection coefficient was below -25 dB. The simulated transmission coefficient varied between -3.1 and -4.88 dB in the same frequency band, as Figure 15b shows. However, the measured transmission coefficient fluctuated between -3 dB and -4.5 dB, with an average difference of approximately 0.45 dB throughout the frequency band and an average insertion loss of 0.002 dB/mm. The double-bend GW-MLW waveguide's measured and simulated performance are compared in Figure 16a,b. The measured reflection coefficient was less than -22 dB, whereas the measured transmission coefficient fluctuated between -3 dB and -5.56 dB, with an average insertion loss of 0.003 dB/mm. The simulated reflection coefficient was less than -30 dB in the lower half and less than -20 dB in the upper half of the frequency band. Moreover, the simulated transmission coefficient stayed around -0.5 dB throughout the entire frequency band.

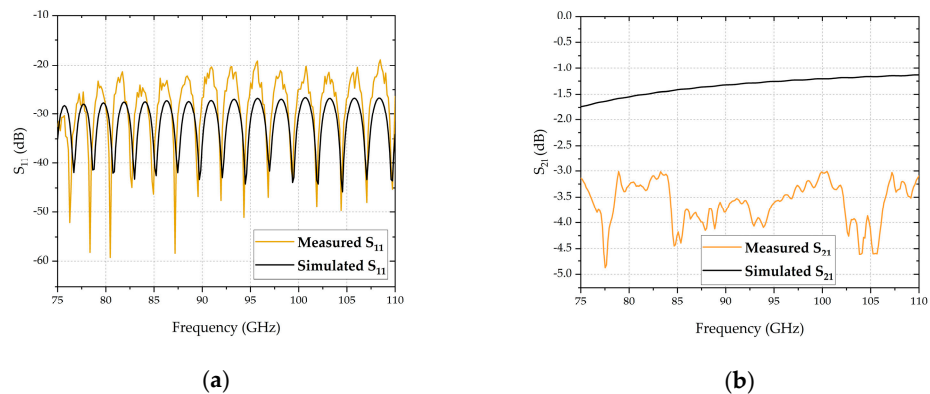


Figure 15. Measured and simulated S-parameters of the W-band straight GW-MLW transmission line. (a) Reflection coefficient. (b) Transmission coefficient.

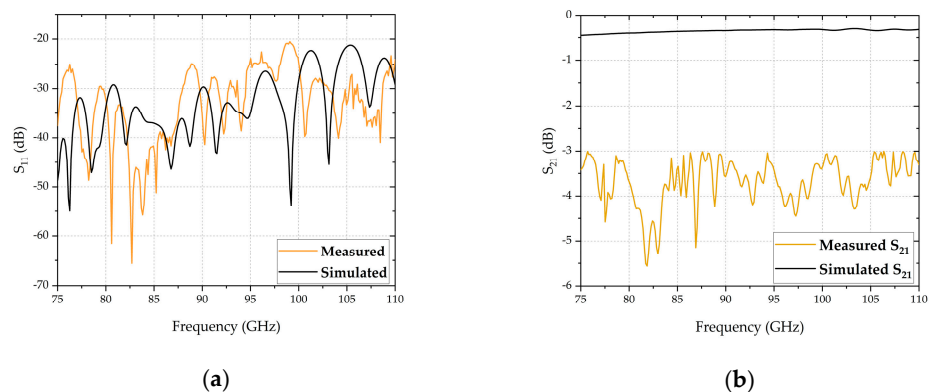


Figure 16. Measured and simulated S-parameters of the W-band double 90° bend GW-MLW transmission line. (a) Reflection coefficient. (b) Transmission coefficient.

4. Discussion

We simulated and manufactured a novel multilayer transmission line that uses walls to prevent field leakage while providing interlocking ability between the layers. The fabricated aluminum W-band GW-MLWs, including straight and double 90° bend configurations, were manufactured using a low-cost chemical metal-etching process. The integrated waveguides consisted of eight stacked layers with additional UG-387/U flange

attachments to provide a connection to the measurement equipment. The prototype was tested using Keysight VNA N5247B. The prototype showed favorable performance regarding reflection and transmission coefficients within the W-band frequency range. The straight waveguide section exhibited a measured reflection coefficient of less than -20 dB, and the measured transmission coefficient fluctuated between -3 dB and -4.5 dB. The double-bend waveguide also exhibited a measured reflection coefficient below -22 dB and a transmission coefficient between -3 dB and -5.56 dB. Fluctuations were observed due to the uncontrolled air gap measurements during testing.

The measured results concluded in Figures 15 and 16 validate the performance of the fabricated prototype. It had decent performance, demonstrating the effectiveness of the proposed waveguide transmission line. Although offering simplicity in design, scalability among different waveguide sizes, and affordability, the multilayered structure was effective in suppressing field leakage and performed as expected. Although the measured results had slightly higher losses than the simulation results, they were due to the differences in conductivity of aluminum in the simulation and measurements and due to fabrication errors and assembly tolerances. The performance of the proposed transmission line can further be improved if materials such as silver and gold, which were shown to have lesser conductivity losses than aluminum, are used inside the waveguide channel in manufacturing. Different interlocking wall configurations can be implemented to further reduce the effects of fabrication and assembly tolerances.

Nonetheless, the proposed architecture has a low profile and low cost and is lightweight. It also does not require the use of dielectric materials. The manufacturing method is the least expensive method, whereby the metals are chemically etched precisely and with high accuracy and can be mass-produced quickly.

Lastly, Table 4 compares several state-of-the-art technologies used for waveguide fabrication and the proposed walled MLW concept. The 3-D printed waveguides have losses comparable to the micromachined waveguides. The waveguides that used chemical etching performed better than the 3-D-printed and micromachined waveguides. The proposed walled structure of multilayer waveguides performed around ten times better than the glide symmetric holey waveguides used in [23] using the same sophisticated and cost-effective manufacturing technology.

Table 4. Comparison between state-of-the-art and proposed waveguide technology.

Ref.	Frequency (GHz)	Split-Block	Technology	Loss (dB/mm)	Simulated/ Measured Loss
This work	75–110 (gold)	H-plane	-	0.0018	Simulated
	110–170 (silver)	H-plane	-	0.0054	Simulated
	75–110 (aluminum)	H-plane (straight)	-	0.002	Simulated
	75–110 (aluminum)	H-plane (bend)	-	0.002	Simulated
	75–110 (aluminum)	H-plane (straight)	MLW (etching)	0.002	Measured
	75–110 (aluminum)	H-plane (bend)	MLW (etching)	0.003	Measured
[23]	110–170 (brass)	H-plane	MLW (etching)	0.02	Measured
[25]	75–110 (copper)	E-plane	3-D printing	0.011	Measured
[26]	110–170 (silicon + gold)	H-plane	Micromachining	0.016	Measured
[35]	110–170 (copper + bronze)	-	3-D printing	0.019	Measured
[36]	110–170 (silver + SU8)	H-plane	Micromachining	0.03	Measured

5. Conclusions

A new transmission line structure for millimeter-wave applications is presented in this paper. The proposed design entails stacking etched metal plates with walls to contain the field within the structure. The simulations were conducted on two bands, namely, the D-band and the W-band, using gold, silver, and aluminum, which demonstrated the structure's scalability to any band and metal. The W-band aluminum model of the simulations was fabricated via chemical metal etching, and lower and upper flange layers were also

manufactured to support the flange fixture, which provided enhanced rigidity in the structure. The walled waveguide channel architecture concept was effective in suppressing field leakages. The prototype's performance measurements supported the proposed idea, and it displayed good agreement between the simulated and measured results. The proposed architecture offers low-loss characteristics, affordability, and simple manufacturability on a mass scale for millimeter-wave applications. The proposed design can serve as a substitute for current multilayer technologies and can be utilized in waveguide components.

Author Contributions: Conceptualization, M.A.S.S.; data curation, M.A.S.S.; formal analysis, M.A.S.S. and Y.Y.; funding acquisition, J.Y.; investigation, M.A.S.S.; methodology, M.A.S.S.; project administration, J.Y.; resources, J.Y. and Y.Y.; software, M.A.S.S.; supervision, J.Y. and Y.Y.; validation, M.A.S.S. and J.Y.; visualization, M.A.S.S.; writing—original draft, M.A.S.S.; writing—review and editing, J.Y., Y.Y. and S.S. All authors have read and agreed to the published version of the manuscript.

Funding: This work was supported in part by the National Natural Science Foundation of China under grant U2241209.

Data Availability Statement: Data is contained within the article.

Acknowledgments: This work was supported by the China Scholarship Council.

Conflicts of Interest: The authors declare no conflicts of interest.

References

1. Rajo-Iglesias, E.; Ferrando-Rocher, M.; Zaman, A.U. Gap waveguide technology for millimeter-wave antenna systems. *IEEE Commun. Mag.* **2018**, *56*, 14–20. [[CrossRef](#)]
2. Vosoogh, A.; Sharifi Sorkherizi, M.; Vassilev, V.; Zaman, A.U.; He, Z.S.; Yang, J.; Kishk, A.A.; Zirath, H. Compact Integrated Full-Duplex Gap Waveguide-Based Radio Front End for Multi-Gbit/s Point-to-Point Backhaul Links at E-Band. *IEEE Trans. Microw. Theory Tech.* **2019**, *67*, 3783–3797. [[CrossRef](#)]
3. Vosoogh, A.; Kildal, P.S.; Vassilev, V. Wideband and High-Gain Corporate-Fed Gap Waveguide Slot Array Antenna with ETSI Class II Radiation Pattern in V-Band. *IEEE Trans. Antennas Propag.* **2017**, *65*, 1823–1831. [[CrossRef](#)]
4. Kildal, P.S.; Alfonso, E.; Valero-Nogueira, A.; Rajo-Iglesias, E. Local metamaterial-based waveguides in gaps between parallel metal plates. *IEEE Antennas Wirel. Propag. Lett.* **2009**, *8*, 84–87. [[CrossRef](#)]
5. Sun, D.; Chen, X.; Deng, J.Y.; Guo, L.X.; Cui, W.; Yin, K.; Chen, Z.; Yao, C.; Huang, F. Gap Waveguide with Interdigital-Pin Bed of Nails for High-Frequency Applications. *IEEE Trans. Microw. Theory Tech.* **2019**, *67*, 2640–2648. [[CrossRef](#)]
6. Ebrahimpouri, M.; Quevedo-Teruel, O.; Rajo-Iglesias, E. Design guidelines for gap waveguide technology based on glide-symmetric holey structures. *IEEE Microw. Wirel. Compon. Lett.* **2017**, *27*, 542–544. [[CrossRef](#)]
7. Ebrahimpouri, M.; Rajo-Iglesias, E.; Sipus, Z.; Quevedo-Teruel, O. Cost-Effective Gap Waveguide Technology Based on Glide-Symmetric Holey EBG Structures. *IEEE Trans. Microw. Theory Tech.* **2018**, *66*, 927–934. [[CrossRef](#)]
8. Santiago, D.; Tamayo-Domínguez, A.; Laso, M.A.G.; Lopetegi, T.; Fernández-González, J.M.; Martínez, R.; Arregui, I. Robust Design of 3D-Printed W-Band Bandpass Filters Using Gap Waveguide Technology. *J. Infrared Millim. Terahertz Waves* **2023**, *44*, 98–109. [[CrossRef](#)]
9. Wu, Y.; Tomura, T.; Hirokawa, J.; Zhang, M. A Wideband Full-Metal Sidewall-Loaded Magnetolectric Dipole Array Based on Combined Ridge and Groove Gap Waveguide in the Q Band. *IEEE Trans. Antennas Propag.* **2023**, *71*, 6156–6161. [[CrossRef](#)]
10. Haghparast, A.H.; Rezaei, P. High performance H-plane horn antenna using groove gap waveguide technology. *AEU—Int. J. Electron. Commun.* **2023**, *163*, 154620. [[CrossRef](#)]
11. Perez-Quintana, D.; Bilitos, C.; Ruiz-Garcia, J.; Ederra, I.; Teniente-Vallinas, J.; Gonzalez-Ovejero, D.; Beruete, M. Fully Metallic Luneburg Metalens Antenna in Gap Waveguide Technology at V-Band. *IEEE Trans. Antennas Propag.* **2023**, *71*, 2930–2937. [[CrossRef](#)]
12. Trinh, T.V.; Park, J.; Song, C.M.; Song, S.; Hwang, K.C. applied sciences A 3-D Metal-Printed Dual-Polarized Ridged Waveguide Slot Array Antenna for X-Band Applications. *Appl. Sci.* **2023**, *13*, 4996. [[CrossRef](#)]
13. Cui, X.; Zhang, B. A Metallic 3D Printed Modularized Dual-Stopband AMC-Loaded Waveguide Slot Filtering Antenna. *Prog. Electromagn. Res. B* **2023**, *100*, 19–38. [[CrossRef](#)]
14. Mahdavi, P.; Hosseini, S.E.; Shojaadini, P. Broadband Three-Section Branch-Line Coupler Realized by Ridge Gap Waveguide Technology from 12 to 20 GHz. *IEEE Access* **2023**, *11*, 46903–46914. [[CrossRef](#)]
15. Hu, L.; Cheng, X.; Li, S.; Wang, C.; Yu, J.; Yao, Y. A High Isolation Duplex Antenna for 79 GHz FMCW Radar System. In Proceedings of the 2023 IEEE International Symposium on Broadband Multimedia Systems and Broadcasting (BMSB), Beijing, China, 14–16 June 2023; pp. 1–2. [[CrossRef](#)]
16. Zhu, L.; Liu, N. Multimode Resonator Technique in Antennas: A Review. *Electromagn. Sci.* **2023**, *1*, 0010041. [[CrossRef](#)]

17. Escobar, A.C.; Mesa, F.; Quevedo-Teruel, O.; Baena, J.D. Homogenization of Periodic Structures Using the Multimodal Transfer Matrix Method. *IEEE Trans. Antennas Propag.* **2023**, *71*, 4976–4989. [[CrossRef](#)]
18. Peng, S.; Pu, Y.; Jiang, Z.; Chen, X.; Wu, Z.; Luo, Y. A Simple Way to Enhance the Isolation of Ridge Gap Waveguide T-Junction, for Application to Millimeter-Wave Feeder Networks. *IEEE Microw. Wirel. Technol. Lett.* **2023**, *33*, 975–978. [[CrossRef](#)]
19. Gonzalez-Gallardo, D.; Algaba-Brazalez, A.; Manholm, L.; Johansson, M.; Quevedo-Teruel, O. Hybrid Glide-Symmetric Unit Cell for Leakage Reduction in Millimeter-Wave PCB Interconnections to Waveguide Components. *IEEE Trans. Microw. Theory Tech.* **2022**, *70*, 2631–2641. [[CrossRef](#)]
20. Alex-Amor, A.; Valerio, G.; Ghasemifard, F.; Mesa, F.; Padilla, P.; Fernández-González, J.M.; Quevedo-Teruel, O. Wave Propagation in periodic metallic structures with equilateral triangular holes. *Appl. Sci.* **2020**, *10*, 1600. [[CrossRef](#)]
21. Alex-Amor, A.; Ghasemifard, F.; Valerio, G.; Ebrahimpouri, M.; Padilla, P.; Gonzalez, J.M.F.; Quevedo-Teruel, O. Glide-Symmetric Metallic Structures with Elliptical Holes for Lens Compression. *IEEE Trans. Microw. Theory Tech.* **2020**, *68*, 4236–4248. [[CrossRef](#)]
22. Blednykh, A.; Kaljuzhny, V.; Lalayan, D.K.M.; Lyapin, A.; Milovanov, O. HOM Damping in a TESLA Cavity Model Using a Rectangular Waveguide. Available online: https://flash.desy.de/reports_publications/tesla_reports/tesla_reports_2000/e1448/infoboxContent1685/tesla2000-34.pdf (accessed on 28 January 2024).
23. Vosoogh, A.; Zirath, H.; He, Z.S. Novel air-filled waveguide transmission line based on multilayer thin metal plates. *IEEE Trans. Terahertz Sci. Technol.* **2019**, *9*, 282–290. [[CrossRef](#)]
24. Tan, W.; He, Y.; Luo, H.; Zhao, G.; Sun, H. Low-Cost Gap Waveguide Technology Using Shallow Grooves and Glide-Symmetric Semicircular-Holes EBG Structures. *IEEE Antennas Wirel. Propag. Lett.* **2023**, *22*, 2901–2905. [[CrossRef](#)]
25. D’Auria, M.; Otter, W.J.; Hazell, J.; Gillatt, B.T.W.; Long-Collins, C.; Ridler, N.M.; Lucyszyn, S. 3-D Printed Metal-Pipe Rectangular Waveguides. *IEEE Trans. Compon. Packag. Manuf. Technol.* **2015**, *5*, 1339–1349. [[CrossRef](#)]
26. Champion, J.; Glubokov, O.; Gomez, A.; Krivovitca, A.; Shah, U.; Bolander, L.; Li, Y.; Oberhammer, J. An Ultra Low-Loss Silicon-Micromachined Waveguide Filter for D-Band Telecommunication Applications. In Proceedings of the 2018 IEEE/MTT-S International Microwave Symposium-IMS, Philadelphia, PA, USA, 10–15 June 2018; pp. 583–586. [[CrossRef](#)]
27. Champion, J.; Li, Y.; Zirath, H.; Oberhammer, J.; Hassona, A.; He, Z.S.; Beuerle, B.; Gomez-Torrent, A.; Shah, U.; Vecchiattini, S.; et al. Toward Industrial Exploitation of THz Frequencies: Integration of SiGe MMICs in Silicon-Micromachined Waveguide Systems. *IEEE Trans. Terahertz Sci. Technol.* **2019**, *9*, 624–636. [[CrossRef](#)]
28. Sanchez-Olivares, P.; Ferreras, M.; Garcia-Marin, E.; Polo-Lopez, L.; Tamayo-Dominguez, A.; Corcoles, J.; Fernandez-Gonzalez, J.M.; Masa-Campos, J.L.; Montejo-Garai, J.R.; Rebollar-Machain, J.M.; et al. Manufacturing Guidelines for W-Band Full-Metal Waveguide Devices: Selecting the most appropriate technology. *IEEE Antennas Propag. Mag.* **2023**, *65*, 48–62. [[CrossRef](#)]
29. Crepeau, P.J.; McIsaac, P.R. Consequences of Symmetry in Periodic Structures. *Proc. IEEE* **1964**, *52*, 33–43. [[CrossRef](#)]
30. Quevedo-Teruel, O.; Valerio, G.; Sipus, Z.; Rajo-Iglesias, E. Periodic structures with higher symmetries. *IEEE Microw. Mag.* **2020**, *21*, 36–49. [[CrossRef](#)]
31. Vosoogh, A.; Uz Zaman, A.; Vassilev, V.; Yang, J. Zero-gap waveguide: A parallel plate waveguide with flexible mechanical assembly for mm-wave antenna applications. *IEEE Trans. Compon. Packag. Manuf. Technol.* **2018**, *8*, 2052–2059. [[CrossRef](#)]
32. Halvaei, B.; Ghalibafan, J.; Rezaee, M. A multi-hole groove gap waveguide directional coupler based on glide-symmetric holey EBG for e-band application. In Proceedings of the 2020 28th Iranian Conference on Electrical Engineering ICEE 2020, Tabriz, Iran, 4–6 August 2020; pp. 5–9. [[CrossRef](#)]
33. Herrán, L.F.; Algaba Brazalez, A.; Rajo-Iglesias, E. Ka-band planar slotted waveguide array based on groove gap waveguide technology with a glide-symmetric holey metasurface. *Sci. Rep.* **2021**, *11*, 8697. [[CrossRef](#)]
34. Lee, S.; Bang, J.; Ahn, B. Design Formulas for Compact Low-Reflection Waveguide Bends. *J. Korean Soc. Inf. Technol.* **2010**, *9*, 89–94.
35. Zhang, B.; Zirath, H. Metallic 3-D Printed Rectangular Waveguides for Millimeter-Wave Applications. *IEEE Trans. Compon. Packag. Manuf. Technol.* **2016**, *6*, 796–804. [[CrossRef](#)]
36. Shang, X.; Yang, H.; Glynn, D.; Lancaster, M.J. Submillimeter-wave waveguide filters fabricated by SU-8 process and laser micromachining. *IET Microw. Antennas Propag.* **2017**, *11*, 2027–2034. [[CrossRef](#)]

Disclaimer/Publisher’s Note: The statements, opinions and data contained in all publications are solely those of the individual author(s) and contributor(s) and not of MDPI and/or the editor(s). MDPI and/or the editor(s) disclaim responsibility for any injury to people or property resulting from any ideas, methods, instructions or products referred to in the content.